Organic–Inorganic Hybrid Composites

DOI: 10.1002/anie.200903234

Flexible Hybrid Semiconductors with Low Thermal Conductivity: The Role of Organic Diamines**

*Xiaoying Huang, Mojgan Roushan, Thomas J. Emge, Wenhua Bi, Suraj Thiagarajan, Jen-Hao Cheng, Ronggui Yang, and Jing Li**

Crystalline compounds built up of periodically ordered nanostructured inorganic semiconductor motifs and organic molecules are a new type of hybrid semiconducting materials that are of great fundamental importance and technological relevance.[1–9] The most appealing feature of these materials is that many favorable properties of each individual component are brought into the hybrid structure by incorporating two distinctly different components into a single crystal lattice. Integration and combination of exceptional transport properties and structural/thermal stability from the inorganic component and superb flexibility and processibility from the organic component can be expected. Additionally, the blending of the inorganic and organic modules in these crystalline hybrid structures takes place at the atomic level and through chemical bonds, and thus is free of the interface issues that are inevitably present in conventional hybrid composite materials. Furthermore, the formation of such hybrid crystals almost always leads to unique and remarkable new features that are not possible for the individual constituents. Some notable examples include organic–inorganic perovskite-like structures and related materials,[1–4] hybrid metal oxides,[5,6] and semiconductors composed of zinc blende and wurtzite frameworks.[7–9]

The II/VI based hybrid semiconductor crystal structures (II: Group 12 elements and Mn; VI: Group 16 elements) are composed of one-dimensional (1D) chains or two-dimensional (2D) slabs of II/VI semiconductor fragments that are interconnected or separated by organic amine molecules to form periodic crystal lattices. They are of the general formula $[MQ(L)_x]$ (M = Mn, Zn, Cd; Q = S, Se, Te; L = organic amine or diamine; and $x = 0.5, 1$). The most intriguing observations include extremely strong band-edge absorption (e.g. 10–20 times higher than bulk II/VI and GaAs) and exceedingly large band-gap tunability (0.1–2.0 eV) as a result of very strong structure-induced quantum confinement.[10–12] Although, according to theoretical calculations,[10] the organic spacers give rise to a very limited effect on the band-gap-related electronic and optical properties, they play a crucial role in the structural, mechanical, and thermal behaviors of these hybrid materials. Herein, we report five crystal structures of 3D-$[ZnTe(L)_{0.5}]$ made of ZnTe single-atomic slabs and long-chain diamines, as well as their structural phase transitions, mechanical properties, specific heat capacity, thermal diffusivity, and thermal conductivity. Our analysis shows that crystalline hybrid semiconductors of this type are much lighter and substantially more flexible than their inorganic counterparts. The incorporation of organic molecules into the semiconductor crystal lattices also leads to significantly reduced thermal conductivity that is most desirable for high performance thermoelectric materials with structural integrity.[13–15]

All the compounds were synthesized by solvothermal reactions using alkyldiamines as reactive solvents (for details, see the Supporting Information). The optimal reaction temperatures were found to be 200–210 °C, and the final products are colorless plate-like crystals; the crystal structures were determined by single-crystal X-ray diffraction methods. α-$[ZnTe(bda)_{0.5}]$ (bda = 1,4-butanediamine; **1**) and α-$[ZnTe(hda)_{0.5}]$ (hda = 1,6-hexanediamine; **3**) are isostructural and crystallized in the orthorhombic space group *Pbca* (Supporting Information, Table S1). Both structures are composed of single-atomic [ZnTe] slabs interconnected via diamine molecules by Zn–N coordinative bonds. Each zinc atom bonds to three tellurium atoms and one nitrogen atom from the alkyldiamine molecule to form a stable tetrahedral conformation. Each tellurium atom connects to three neighboring zinc atoms. Alternating zinc and tellurium atoms form puckered six-membered rings extended in two dimensions (the crystallographic *ab* plane). The overall three-dimensional structures of **1** and **3** are given in Figures 1a and 2a, respectively. The $[ZnTe(ptda)_{0.5}]$ structure (ptda = 1,5-penta-

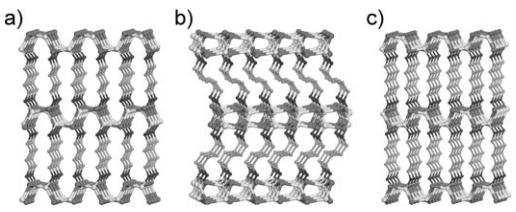

Figure 1. a) α-$[ZnTe(bda)_{0.5}]$ (**1**), b) γ-$[ZnTe(bda)_{0.5}]$ (**1a**), c) $[ZnTe(ptda)_{0.5}]$ (**2**). Small spheres: C light gray, N dark gray; large spheres: Zn light gray, Te dark gray.

[*] Dr. X. Huang,[+] M. Roushan,[+] Dr. T. J. Emge, Dr. W. Bi, Prof. J. Li
Department of Chemistry and Chemical Biology,
Rutgers, The State University of New Jersey
Piscataway, NJ 08854 (USA)
Fax: (+1) 732-445-5312
E-mail: jingli@rutgers.edu
S. Thiagarajan, J.-H. Cheng, Prof. R. Yang
Department of Mechanical Engineering,
University of Colorado at Boulder
Boulder, CO 80309 (USA)
[+] These authors contributed equally.

[**] The authors are grateful for the financial support from NSF (Grant No. DMR-0706069).

Supporting information for this article is available on the WWW under http://dx.doi.org/10.1002/anie.200903234.

nediamine; **2**) belongs to an orthorhombic non-centrosymmetric space group $Cmc2_1$. The local environment of zinc atoms and tellurium atoms and the overall structural connectivity in **2** are similar to that in **1** and **3** (see Figure 1c). δ-[ZnTe(*hda*)$_{0.5}$] (**4**) crystallizes in the chiral space group[16] $P2_12_12_1$ with a five-fold commensurate supercell (here 5*b*) with a *c* axis that is shorter by about 2 Å compared to that of **3**. There are ten zinc atoms, ten tellurium atoms, and five hda molecules in one asymmetric unit of **4**. As shown in Figure 2c, the local environment (that is, the bonding between zinc and

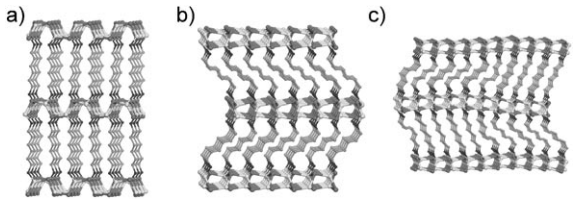

Figure 2. The three structural forms of three-dimensional [ZnTe(hda)$_{0.5}$]: a) α-[ZnTe(hda)$_{0.5}$] (**3**), b) γ-[ZnTe(hda)$_{0.5}$] (**4a**), c) δ-[ZnTe(hda)$_{0.5}$] (**4**).

tellurium atoms) of the inorganic ZnTe slabs in **4**, and the connectivity between the ZnTe slabs and hda molecules, are similar to that of **3**. The difference lies in the conformation of the hda molecules. In **3**, the five C–C bonds of hda are all *trans* (*T*), namely *TTTTT* (Supporting Information, Figure S1). This is in contrast to **4**, where two of the five crystallographically independent hda molecules have the *all-trans* (*TTTTT*) conformation, the other three take alternate conformations *GTTTG* and *GTGTT* (mixture of *trans* (*T*) and *gauche* (*G*)). Note that the linear extent of the hda molecules vary from about 10.3 Å (*TTTTT*) to circa 9.5 Å (*GTGTT*) and to about 9.2 Å (*GTTTG*). Consequently, the shortest interlayer distance between the adjacent inorganic ZnTe slabs is 6.25 Å in **4** (using the covalent radius of tellurium), and 8.12 Å in **3**.

Interestingly, **1**, **3**, and **4** underwent phase transitions at various temperatures. Upon slow cooling from room temperature to 100 K, **1** transformed into γ-[ZnTe(bda)$_{0.5}$] (**1a**; Figures 1b). Both **3** and **4** are stable at room temperature, but single crystals of **3** rarely survive multiple fractures during the initial cooling from the synthesis at 473 K. However, single crystals of **3** can be reliably produced by slow heating of **4** to above room temperature, and once formed, they remain stable upon cooling slowly to room temperature. The unit cell parameters from single-crystal X-ray data show that **3** or **4** transforms to γ-[ZnTe(hda)$_{0.5}$] (**4a**; Figure 2b) upon slow cooling to 100 K. However, upon subsequent slow warming to room temperature, **4a** only transforms into **4**. The phase transition temperatures were determined to be about 130 K for **1**→**1a** and about 225 K for **4**→**4a**, respectively, based on DSC measurements (Supporting Information, Figure S5). These transitions were also found to be reversible by measuring lattice parameters of a selected crystal following a cooling and heating cycle well below and above the transition temperature. The low-temperature γ phases **1a** and **4a** also belong to the *Pbca* space group; therefore, their overall structures are similar to those of the corresponding α phases. However the conformations and site symmetries of the diamine molecules are different. Instead of an *all-trans* form in **1** and **3**, the diamine molecules in **1a** and **4a** adopt the *GTG* and *GTTTG* configurations, respectively, which results in shorter diamine lengths and thus shorter interlayer distances between the adjacent inorganic slabs compared to the corresponding α phases (Supporting Information, Table S2). It is worth noting that the structure transition between **3** and **4** occurs at temperatures slightly higher than room temperature, and **2** does not undergo a structural transformation at low temperatures (room temperature–100 K). Crystal data obtained at 100 K confirmed that the structure remained unchanged (denoted as **2a**). In fact, phase transitions have only been observed for three-dimensional [ZnTe(L)$_{0.5}$] structures in which the ligand L possesses an even number of carbon atoms (centric and polar, with *i* site symmetry). No phase transitions are found for those having L with an odd number of carbon atoms (acentric and polar, with *m* site symmetry).

The optical bandgaps of **1**, **2**, and **4** were estimated from the diffuse reflectance experiments conducted on polycrystalline samples. The values are about 3.5 eV for all three compounds (Supporting Information, Figure S7). As expected, these compounds exhibit a very large blue shift (ca. 1.4 eV) in their optical absorption edge compared to the bandgap of bulk ZnTe (2.1 eV), as a consequence of structure-induced quantum confinement.[7,9]

The title compounds are significantly lighter than their inorganic counterpart ZnTe (Supporting Information, Table S3), and appear to be highly flexible based on their crystal structures.

To assess the mechanical properties of the compounds, we carried out a compression experiment on selected samples. The powder samples were pressed into thin pellets (disks) of 13 mm in diameter and 0.5–0.8 mm in thickness using a Caver laboratory press under a load of 3.8 tons (2500 atm pressure). The stress/strain data in the low pressure range are shown in Figure 3 for [ZnTe(L)$_{0.5}$], with L = hdz (hydrazine; N_2H_4), en (ethylenediamine),[7] pda (propanediamine),[7] bda, and hda, along with three reference samples, ZnTe, pentacene, and polystyrene prepared in the same manner. From the graph, it

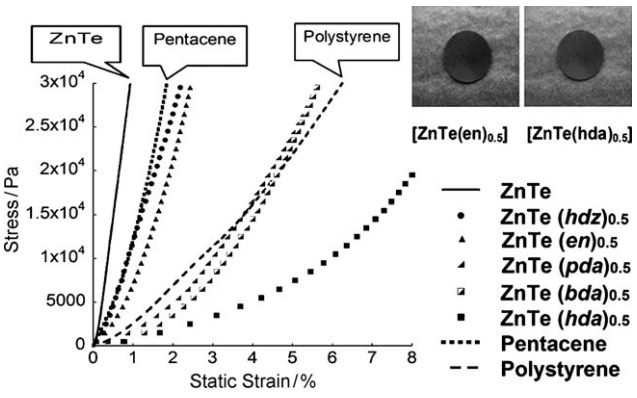

Figure 3. Stress–strain plots for the α-[ZnTe(L)]$_{0.5}$-type hybrid structures in comparison with three reference materials. Insets: two pellets.

is obvious the hybrid structures having shorter amine ligands show similar behavior as the organic pentacene, whereas those with longer amines fall in the same range as polystyrene. [ZnTe(hda)$_{0.5}$], which has the longest diamine, shows significantly larger strain than polystylene under the same pressure (stress). Compared to the behavior of the parent semiconductor compound ZnTe, it is clear that the introduction of the organic linear amines leads to a significant increase in the strain and deformation; the materials become less brittle and more flexible. The highly flexible nature of these hybrid structures is also evident from the free-standing film samples (Figure 4).

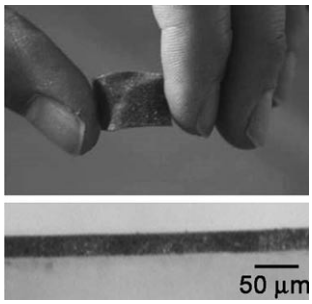

Figure 4. Top: A free-standing film specimen made from a powder sample of [ZnTe(hda)$_{0.5}$]. Bottom: side view of the film. The thickness of the film is about 25 μm.

The thermal conductivity of selected [ZnTe(L)$_{0.5}$] samples was determined by separately measuring the density, specific heat capacity, and thermal diffusivity. The results of the thermal conductivity measurements are shown in Figure 5. All the hybrid samples have thermal conductivity considerably lower than that of a ZnTe sample prepared by the same cold-pressing process. It is clear that the addition of the organic molecules of increasing length (from N_2H_4 to en to pda) to the ZnTe structure leads to a corresponding increase in unit cell length of the resultant hybrid compounds. This, in turn, gives rise to a monotonic increase in specific heat

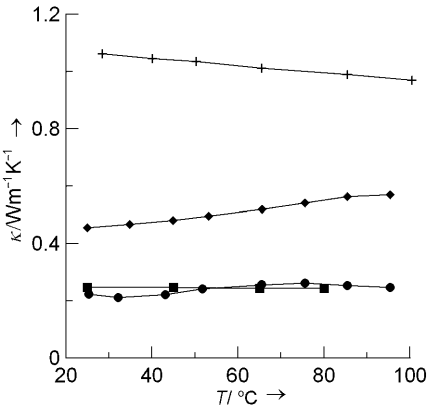

Figure 5. Thermal conductivity plots for hybrid structures ZnTe-$(N_2H_4)_{0.5}$ (◆), ZnTe(en)$_{0.5}$ (■), and ZnTe(pda)$_{0.5}$ (●) in comparison with ZnTe reference material (+).

(Supporting Information) and a reduction of the thermal conductivity as a consequence of introducing organic–inorganic interfaces at the atomic scale.[17,18] The increase in the specific heat capacity of the hybrid samples (Supporting Information, Figure S8), coupled with a slight decrease in the thermal diffusivity (Supporting Information, Figure S9) leads to a net increase in the thermal conductivity with temperature, whilst in the case of ZnTe, the specific heat stays nearly constant and the diffusivity decreases with temperature, resulting in a net decrease. We note that the thermal conductivity of the cold-pressed ZnTe sample is lower than data reported elsewhere, which is possibly due to the lack of good thermal contact between the grains.[19] Nevertheless, such an error is systematically transformable, and the difference obtained from the thermal conductivity data clearly show a decrease of nearly an order of magnitude going from ZnTe to hybrid structures.

In summary, we have demonstrated that a unique type of inorganic–organic hybrid semiconductor material built on covalently bonded ZnTe single-atomic slabs and long-chain organic alkyldiamines is significantly lighter and more flexible than the inorganic parent structure. The thermal conductivity of the hybrid samples is considerably lower than ZnTe prepared using a similar processing route. Utilization of hybrid semiconductors of this type in low-weight and flexible optoelectronic devices may well become a future possibility.

Experimental Section

ZnF_2 (99%, Alfa Aesar), $Zn(NO_3)_2{\cdot}6H_2O$ (97%, Alfa Aesar), Te (99.5%, Strem), 1,4-butanediamine (bda, 99%, Alfa Aesar), 1,5-pentanediamine (ptda, 95%, TCI), 1,6-hexanediamine (hda, 98%, Alfa Aesar) were used in the synthesis as received without further purification. Single-crystal X-ray diffraction data in the temperature range 100 K to 400 K were collected on an automated Enraf–Nonius CAD4 diffractometer or Bruker-AXS Smart APEX CCD diffractometer with graphite monochromated $Mo_{K\alpha}$ radiation ($\lambda =$ 0.71073 Å). Powder X-ray diffraction (PXRD) analysis of polycrystalline samples was performed on a Rigaku D/M-2200T automated diffraction system (Ultima$^+$). Optical diffuse reflectance spectra were measured at room temperature using a Shimadzu UV-3101PC double-beam, double-monochromated spectrophotometer. Differential scanning calorimetry (DSC) was performed on a DSC 2920 thermal analyzer (TA instruments). Compression experiment was carried out on pellet samples using a PE DMA 7e system with TAC 7/DX instrument controller. Data analysis was made using PE Pyris software (v3.81). Thermal diffusivity measurements were carried out using laser flash apparatus LFA 457 Microflash (Netzsch Instruments) and specific heat measurements were made using DSC 204F1 (Netzsch Instruments). CCDC 736292–CCDC 736298 contain the supplementary crystallographic data for this paper. These data can be obtained free of charge from The Cambridge Crystallographic Data Centre via www.ccdc.cam.ac.uk/data_request/cif.

Received: June 15, 2009
Revised: August 1, 2009
Published online: September 10, 2009

Keywords: heat capacity · phase transitions · semiconductors · structure isomorphs · thermal conductivity

[1] C. R. Kagan, D. B. Mitzi, C. D. Dimitrakopoulos, *Science* **1999**, *286*, 945.
[2] D. B. Mitzi in *Progress in Inorganic Chemistry*, *Vol. 48* (Ed.: K. D. Karlin), Wiley, New York, **1999**, p. 1.
[3] D. B. Mitzi, C. R. Kagan in *Thin-Film Transistors* (Eds.: C. R. Kagan, P. Andry), Marcel Dekker, New York, **2003**, p. 475.
[4] T. Ishihara in *Optical properties of Low-Dimensional Materials*, *Vol. 1* (Eds.: T. Ogawa, Y. Kanemitsu), World Scientific, Singapore, **1996**, p. 289 – 335.
[5] J. W. Johnson, A. J. Jacobson, S. M. Rich, J. F. Brody, *J. Am. Chem. Soc.* **1981**, *103*, 5246.
[6] B. B. Yan, Y. Xu, N. K. Goh, L. S. Chia, *Chem. Commun.* **2000**, 2169.
[7] X. Y. Huang, J. Li, H. Fu, *J. Am. Chem. Soc.* **2000**, *122*, 8789.
[8] X. Y. Huang, H. R. Heulings IV, V. Le, J. Li, *Chem. Mater.* **2001**, *13*, 3754.
[9] X. Y. Huang, J. Li, Y. Zhang, A. Mascarenhas, *J. Am. Chem. Soc.* **2003**, *125*, 7049.
[10] H. Fu, J. Li, *J. Chem. Phys.* **2004**, *120*, 6721.
[11] B. Fluegel, Y. Zhang, A. Mascarenhas, X. Y. Huang, J. Li, *Phys. Rev. B* **2004**, *70*, 205308.
[12] Y. Zhang, G. M. Dalpian, B. Fluegel, S. H. Wei, A. Mascarenhas, X.-Y. Huang, J. Li, L.-W. Wang, *Phys. Rev. Lett.* **2006**, *96*, 026405.
[13] M. S. Dresselhaus, G. Chen, M. Y. Tang, R. G. Yang, H. Lee, D. Z. Wang, Z. F. Ren, J. P. Fleurial, P. Gogna, *Adv. Mater.* **2007**, *19*, 1043.
[14] H. J. Goldsmid, *Thermoelectric Refrigeration*, Plenum, New York **1964**.
[15] D. M. Rowe, *Thermoelectrics Handbook: Macro to Nano*, CRC, Boca Raton, **2005**.
[16] S. W. Ng, S. Z. Hu, *Chin. J. Struct. Chem.* **2003**, *22*, 37.
[17] G. Chen, D. Borca-Tascuic, R. G. Yang in *Encyclopedia of Nanoscience and Nanotechnology*, *Vol. 7* (Eds.: H. S. Nalwa), American Scientific Publishers, New York, **2004**, pp. 429 – 459.
[18] D. G. Cahill, W. K. Ford, K. E. Goodson, G. D. Mahan, A. Majumdar, H. J. Maris, R. Merlin, and S. R. Phillpot, *J. Appl. Phys.* **2003**, *93*, 793.
[19] L. Berger, Semiconductor Materials, CRC, Boca Raton, **1996**.

